Picosecond laser welding of similar and dissimilar materials

Carter, Richard; Chen, Jianyong; Shephard, Jonathan D; Thomson, Robert R; Hand, Duncan Paul

Published in:
Applied Optics

DOI:
10.1364/AO.53.004233

Publication date:
2014

Picosecond laser welding of similar and dissimilar materials

Richard M. Carter,* Jianyong Chen, Jonathan D. Shephard, Robert R. Thomson, and Duncan P. Hand

Institute of Photonics and Quantum Sciences, Heriot-Watt University, Edinburgh, EH11 4AS, UK

*Corresponding author: r.m.carter@hw.ac.uk

Received 24 February 2014; revised 15 April 2014; accepted 12 May 2014; posted 29 May 2014 (Doc. ID 206734); published 30 June 2014

We report picosecond laser welding of similar and dissimilar materials based on plasma formation induced by a tightly focused beam from a 1030 nm, 10 ps, 400 kHz laser system. Specifically, we demonstrate the welding of fused silica, borosilicate, and sapphire to a range of materials including borosilicate, fused silica, silicon, copper, aluminum, and stainless steel. Dissimilar material welding of glass to aluminum and stainless steel has not been previously reported. Analysis of the borosilicate-to-borosilicate weld strength compares well to those obtained using similar welding systems based on femtosecond lasers. There is, however, a strong requirement to prepare surfaces to a high (10–60 nm Ra) flatness to ensure a successful weld.

OCIS codes: (170.0110) Imaging systems; (170.3010) Image reconstruction techniques; (170.3660) Light propagation in tissues.

http://dx.doi.org/10.1364/AO.53.004233

1. Introduction

Microjoining, and in particular microwelding, are important manufacturing techniques in a variety of industries [1–4]. Various methods, including adhesive bonding, fusion bonding, arc bonding, anodic bonding, soldering, and frit, have been developed to manufacture MEMS, microfluidic and micro-optical devices, particularly in the field of sensors. Laser microwelding has seen an increase in interest in recent years as it provides advantages of high precision, high speed, small thermally affected zone while eliminating the effect of creep, out-gassing, and any undesirable materials commonly found with interlayer techniques. Laser microwelding allows the direct bonding of two materials [5–9].

To date most research has focused on the use of femtosecond [5,6,8,10–16] or nanosecond [6] pulses for weld creation in optically transparent similar materials, with picosecond pulse techniques only recently being developed [17–20]. The advantage of short pulsed laser systems is the ability to place the optical absorption region in the bulk of the material through nonlinear interactions at the focus. This creates a heated zone that is highly localized to the material join, which is critical for the joining of two transparent materials. Through melting or microplasma generation any small gap between the materials is effectively filled and a solid join created [5,9].

In contrast, when welding a transparent to a non-transparent material [e.g., fused silica (SiO_2)–metal] the principal absorption process is linear at the metal–glass interface [6]. This reduces the precision required in the placement of the focal depth of the laser while maintaining a small heat affected zone but requires one of the joined materials to be transparent.

This small heat affected zone allows for the welding of dissimilar materials by limiting the impact of the differential thermal expansion experienced by the two materials. To date this has been demonstrated with femtosecond laser systems welding fused silica to Cu [6] and Si [14].

1559-128X/14/194233-06$15.00/0

While localized welding is possible with high-power single shot systems [9], fast efficient melting or microplasma generation in these materials generally requires thermal accumulation from multiple laser pulses. This in turn requires a high repetition rate such that the arrival of the next pulse occurs before the thermal energy of the previous pulse is dissipated. This dissipation is of the order of microseconds and thus a repetition rate of the order of 100 s kHz facilitates thermal accumulation [7].

2. Laser Welding Setup

The key challenge in laser microwelding is to bring the two materials into sufficiently close contact that they are both within the effective focal depth of the laser and can confine the plasma once generated. Too large a gap between the two materials allows the plasma to escape and ablation, rather than a weld results [9]. This effectively requires an area of optical contact (which can be defined as the clear spot in the center of a set of Newton's rings [5,9]). With two perfectly clean, perfectly flat surfaces this can be readily achieved by simply placing one material on top of the other. For a more realistic material—and nonclean room environment—it is necessary to force the two materials together. Once forced into optical contact, Van der Waals forces are generally capable of holding together the two materials [12] provided they are of a minimum smoothness (and flatness).

These levels of flatness are readily achievable with most materials if sufficient care is taken to lap or polish the surfaces. Additionally, $\lambda/4$ flatness has become an industry standard for the preparation of optical glasses.

For the purposes of this paper, proof-of-principle demonstrations have been carried out using polished metal samples. These samples were polished in stages down to 1 μm diamond suspension, producing a mirror finish with an Ra of ~10 nm or 60 nm in Al. Glasses and sapphire have been purchased with $\lambda/4$ flatness and silicon wafer with surface roughness, Ra, of <5 nm.

In all cases the two materials were clamped together during the welding process by use of a four-point loading system (Fig. 1); this process is similar to those reported previously (e.g., [5,6,9,13]). This creates an area of optical contact in line with the central loading position, and the incident laser radiation, directly above the piston. In an idealized setup, a scan head would be used to scan the required weld geometry; however, a scan head with a sufficiently small focal length (~10 mm, giving a spot size of 1.2 μm) was not readily available. Instead the sample clamp is mounted on x,y,z translation stages which move the sample through the fixed focus of the laser (Aerotech pro115 with ~6 μm accuracy).

The incident radiation is focused through a 10 mm focal length lens (NA 0.5) onto the glass–glass interface. This interface can be found by monitoring the CCD (Fig. 2). This CCD has no focussing optic, a Fresnel reflection from an interface will therefore

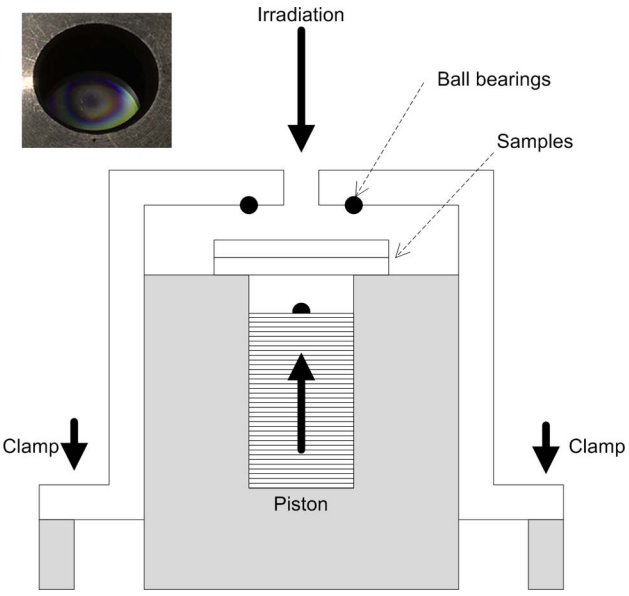

Fig. 1. Schematic for the point loading system used to create optical contact between samples. The pneumatically actuated piston provides force to create an area of optical contact (insert) over the central piston.

be focused onto the CCD by the welding objective when the system is focused slightly above the interface. This offset is a constant for a given lens and collimation, and can be readily measured by finding the offset between apparent (CCD) focus and true (plasma threshold) focus on the air–glass interface. Since the two glass plates are in optical contact there is no Fresnel reflection from this interface. Instead the system was focused onto the first air/glass interface and then translated by an amount calculated based on the glass thickness and refractive index to focus onto or just below the join within ~10 μm. In the case of glass–metal welding there is a reflection from the interface but the above method was applied for consistency.

Figure 2 illustrates the optical train from the 1030 nm laser (Trumpf Tru Micro 5 × 50) to the sample. The laser is capable of altering the peak power of the pulses without changing the pulse shape but the minimum peak power is only slightly less than is required for the welding process. In order to provide finer control of the peak pulse power, a half-wave plate and polarizing beam splitter are used to reduce

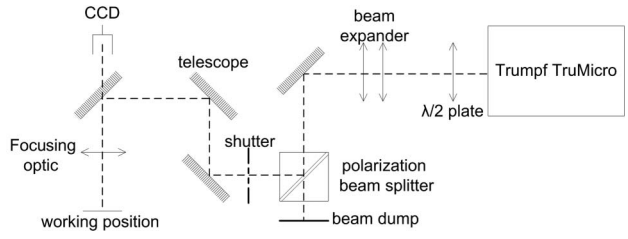

Fig. 2. Optical train for welding system. The beam expander increases the beam diameter from 5 mm FWHM to 10 mm FWHM, while the half-wave plate and polarizing beam splitter provide rough power selection.

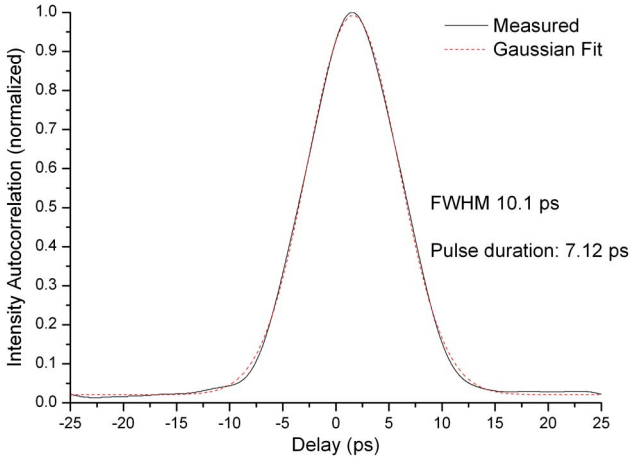

Fig. 3. Autocorrelation of pulse envelope of ps laser used.

the (linearly polarized) beam power by a factor of 25. Beam on/off control is provided by the shutter (Fig. 2), which is coordinated with the stage controls. In all cases the repetition rate and pulse shape are the same: 7.12 ps (Gaussian fit, Fig. 3) at 400 kHz. The average power (measured as incident power at the workpiece) is therefore the only variable between materials.

The chosen weld pattern is an outward arithmetic spiral (Fig. 4). This pattern allows a single continuous weld seam to be drawn with no corners to accumulate stress. The weld process is started at a slight offset to the center of the weld pattern—but in the center of the area of optical contact. In all cases the pattern has a pitch of 0.1 mm, a final radius of 1.25 mm, and is translated at 1 mm s^{-1}.

3. Weld Strength Measurement

To test the strength of the glass-to-glass welds, a simple shear test method was developed. Two differentially sized pieces of glass were welded together using a guide to ensure the glass is parallel and correctly aligned. This fits into the recesses in the sliding block arrangement in Fig. 5.

The two sides of the block are pulled apart using an Instron 3367 at a rate of 30 μm s^{-1} with the applied force recorded as a function of the extension. The maximum force, which occurs immediately before breakage, minus the residual weight offset of the block device (Fig. 6) is used to determine the weld breaking stress.

The analysis of the facture strength of glass is complex. Glass fails by brittle fracture and is dependent on the distribution of flaws within the test volume. Consequently it is necessary to take multiple measurements of the same weld parameter and statistically analyze them to determine the probability of failure for a given stress. In this case, a Weibull function [Eq. (1)] [21] was fitted to the weld fail probabilities over 20 samples. Due to time constraints one set of welding parameters was tested: 1.79 W at 1 mm s^{-1}. This was chosen such that the lateral heat affected zone (i.e., weld) is 0.1 mm wide to match the pitch of the weld pattern, forming a continuous and complete weld. The weld area is thus a circle of diameter 2.5 mm:

$$P_s(V_0) = \mathrm{Exp}\left[-\left(\frac{\sigma}{\sigma_0}\right)^m\right], \tag{1}$$

where P_s is the probability of survival for a given parameter (i.e., strain), σ is the parameter, σ_0 is the strain for $1/e$ survivability, and m is the Weibull modulus.

This measurement provides a comparable reference with other, similar published data. Since the

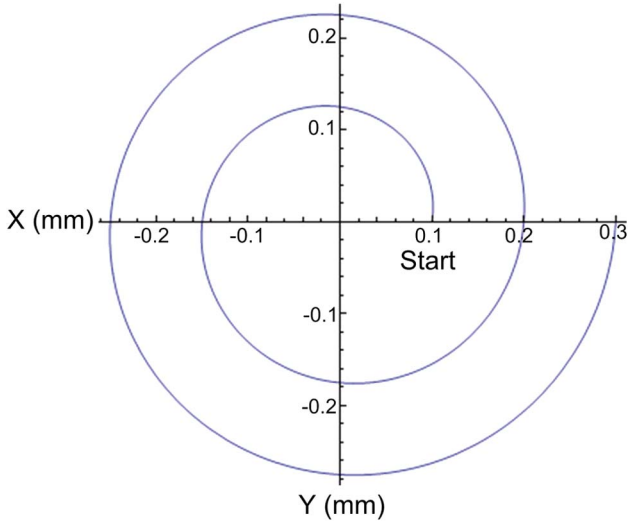

Fig. 4. Diagram of weld pattern used. The pattern is an outward arithmetic spiral with a pitch of 0.1 mm. The start position is offset from the spiral center by 0.1 mm (i.e., 2π). The spiral continues to a maximum radius of 1.25 mm (not shown).

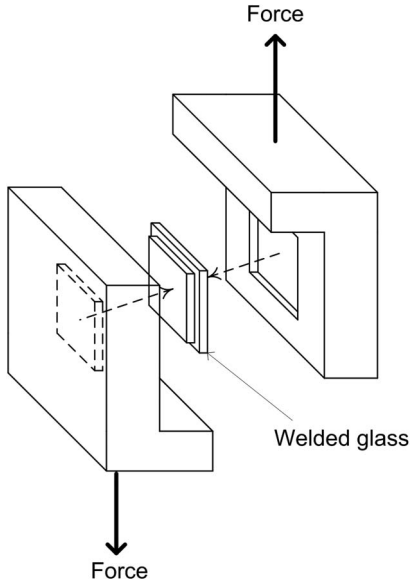

Fig. 5. Exploded view of shear break testing rig. Two differentially sized pieces of glass fit into machined recesses in an aluminum block. The block is loosely held with sliding bolts (not shown) and pulled apart along an axis normal to the weld plane.

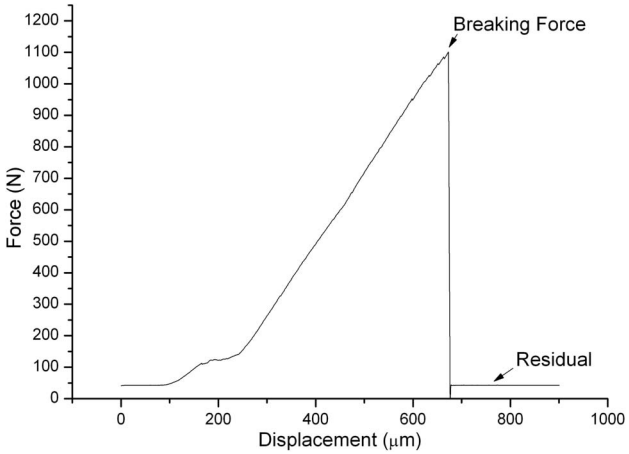

Fig. 6. Example plot of recorded shear force test. The shear force for the piece is calculated as the breaking force minus the residual force (due to the mass of the test rig being supported by the mechanism).

weld fracture in both similar and dissimilar welding occurs around the weld in the bulk glass it is to be expected that weld strengths of the dissimilar materials will be similar.

4. Results

Figure 7 shows examples of successful welding of one transparent and one opaque, dissimilar material, namely fused silica and borosilicate to aluminum, copper, and stainless steel at 1.15 W, to silicon (1.15 W) and sapphire to stainless steel (4.5 W). In all cases linear rather than nonlinear absorption is required and as a result the average power required for each pair of materials does not vary considerably.

The stainless steel examples show cracking at the weld edges. These cracks have formed at the metal–glass interface but propagated only 100–200 μm into the glass before self-terminating. We believe that these are formed due to the comparatively low thermal conductivity of stainless steel. This results in a steeper thermal gradient across the weld seam than with the other metals. The material is bonded together with this steep thermal gradient in place.

Once the sample cools, this high thermal gradient translates to a high stress gradient, which results in the formation of microcracks.

The resultant weld seams are continuous (with visible backlash due to the stages) and are highly scattering (i.e., black under standard microscopy). Dark field microscopy reveals a two-layer feature to the weld seams [Figs. 8(C) and 8(D)]. The outer seam is ~40 μm and corresponds to the weld visible with standard, bright field microscopy. Inside this, however, is an inner seam of approximately half the width (~20 μm).

An example of aluminum to borosilicate welding was cut with a diamond saw and side-polished to view the weld cross section [Figs. 8(A) and 8(B)].

The sample cracked as a result of the polishing applied to the sample. This side-polished example

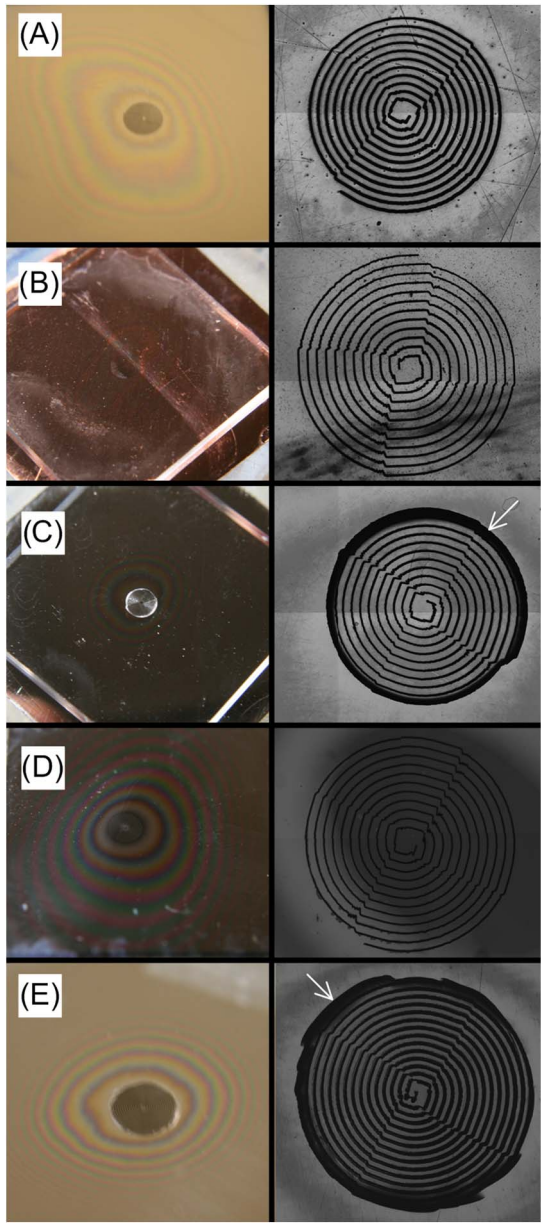

Fig. 7. Photographs (left) and microscope images (right) of: (A) Al to SiO_2, (B) Cu to SiO_2, (C) stainless steel to borosilicate, (D) Si to SiO_2, and (E) sapphire to stainless steel. White arrows indicate cracking in stainless steel examples.

provides an explanation for the apparent double seam seen in dark field imaging. The outer region represents the width of the modified glass region while the inner region indicates the width of the modified aluminium. An electron microscope with XPS spectroscopy was used to determine that the weld volume is a true mix of aluminum, silicon and oxygen, which is to be expected following re-solidification from an intermediate plasma volume (Fig. 9). Here it is possible to see that the smaller, inner weld seam of 20 μm comprises of a mix of Al and Si with penetration of both into the opposite media. The larger visible seam appears to be made of only Si and O. This is quite consistent with the

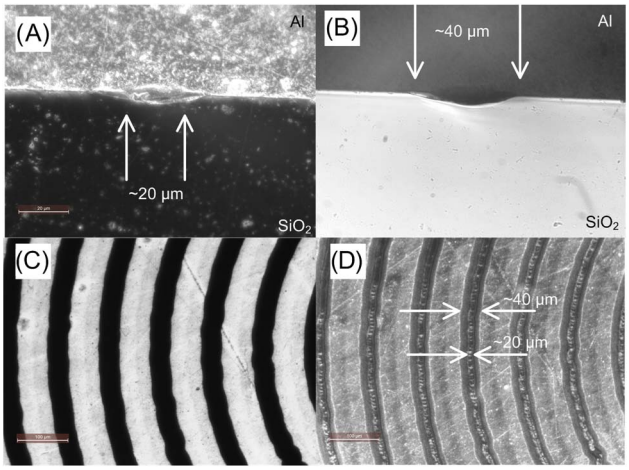

Fig. 8. Microscopy images of aluminum to SiO_2 weld. (A) Dark field side-polished view at 100×, (B) transmission side-polished view at 100×, (C) bright field image at 20×, and (D) dark field image at 20×.

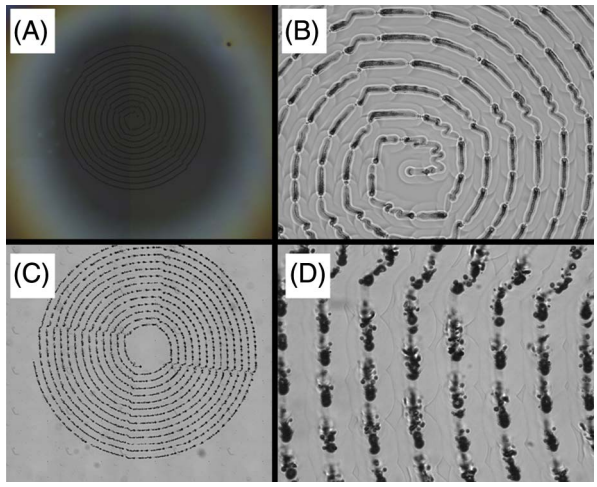

Fig. 10. Microscope images for borosilicate to borosilicate welding: (A) overview (reflection 5×), (B) detail (transmission 20×) and fused silica to fused silica welding, (C) overview (reflection 5×), and (D) detail (transmission 20×).

expectation that the plasma-weld volume would be surrounded by a region of modified glass, which while optically visible and bonded to the Al surface does not form a true weld.

Figure 10 shows the welding to two transparent materials, fused silica to fused silica (2.35 W) and borosilicate to borosilicate (1.59 W). The average power requirements for welding are higher than for the opaque materials due to the lack of linear absorption. Higher magnification views of the weld region shows a "pulsed" weld formation, which is to be expected from previous studies of laser-induced glass modification [20,22].

Due to the difficulties in material preparation—in this case the polishing process produces a smooth but nonflat bowed surface—we have been unable to analyze the weld strength for opaque to transparent materials properly; however, a single measurement of aluminum to borosilicate was attempted on a Nordson Dage 4000 Series Bondtester giving a shear fracture strain of 113.6 N mm^{-2}.

A more comprehensive set of tests was carried out to determine the weld bond strength of borosilicate-to-borosilicate welds. As outlined above (Section 3), one set of parameters was tested, 1.79 W. Figure 11 shows the Weibull plot for these results taken across 20 samples. The long tail on the Weibull plot from 1000–2000 N mm^{-2} is an indication of the effect of Van der Waals forces. Samples with larger regions of optical contact will be reinforced by this effect.

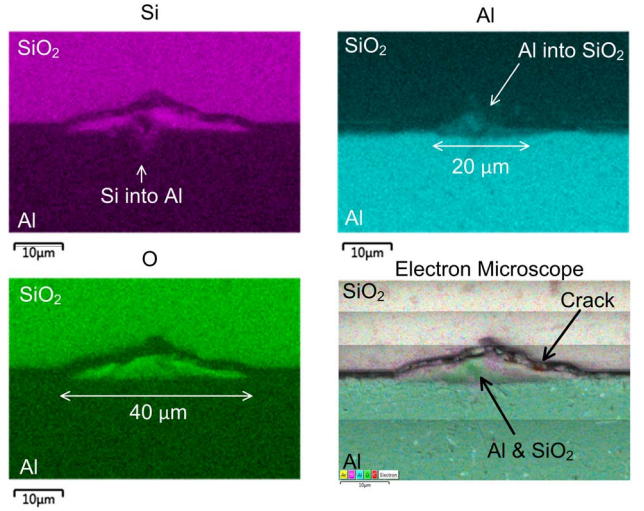

Fig. 9. Electron microscope and XPS analysis of Al-SiO_2 weld showing a mix of Al, Si, and O in the weld region. Note that the glass has cracked during cutting and polishing outside of the weld region.

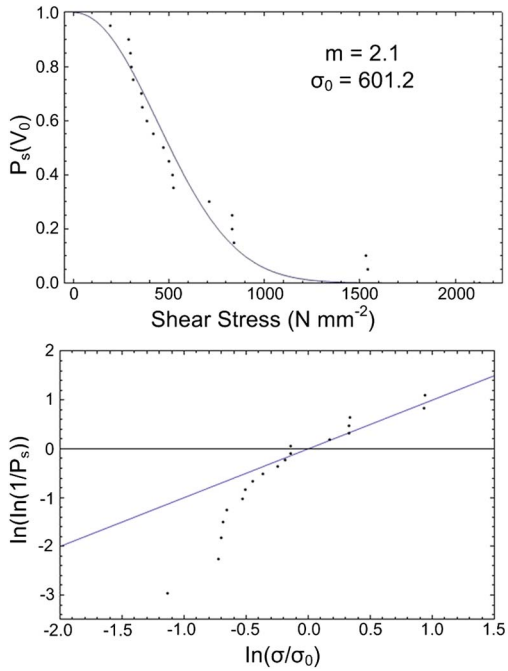

Fig. 11. Weibull plots for borosilicate-to-borosilicate weld shear tests based on a series of 20 1.79 W, Ø 2.5 mm welds.

As the samples were not prepared in a clean room the area of optical contact is extremely difficult to control and varies from sample to sample. The highest strength welds were observed to have significantly larger areas of optical contact, up to 200 mm^{-2}. It is not possible to adequately control or compensate for this additional force. The precise separation of the glass plates cannot be measured or estimated and has a critical effect on the size of the Van der Waals force. This additional force component simply adds to the statistical spread of the failure test and manifests as a low Weibull modulus.

Based on the Weibull plot, the 90% and 99% survival stresses are 206.6 $N\,mm^{-2}$ and 67.5 $N\,mm^{-2}$, respectively, which is larger than comparative adhesives (~10–20 $N\,mm^{-2}$ [23]). The mean failure (σ_0) is 601.2 $N\,mm^{-2}$, which compares favorably with similar femtosecond laser welds of 5–400 $N\,mm^{-2}$ [6–8,10–12,15,16,18,19].

5. Conclusions

The versatility of this welding process is aptly demonstrated by the range of materials that can be welded together under essentially the same laser parameters. Welding of aluminum and stainless steel to glass and sapphire has been demonstrated for the first time. Given the diverse thermal properties of these materials it is to be expected that a considerably larger range of materials can be welded together using this process.

Since our metal surface preparation leaves it embedded in a resin block and provides a smooth but not flat surface it has not been possible to comprehensively test the weld strength of the opaque to transparent welds. However, it should be noted that in all cases the welds fractured around the modified region within the glass. The weld strengths for opaque to transparent materials are therefore expected to be similar to those for transparent–transparent material welding. Nevertheless we believe that this demonstrated the versatility and potential of this system.

The main limit, currently, to implementation of this method is the requirement on the smoothness and flatness of the surfaces; however, the relatively large weld strengths recorded indicate that it may be necessary to only weld, and therefore surface process, small areas to achieve a suitably strong weld. Continuing work in this area will concentrate on a reproducible, robust, and versatile method for surface preparation, which is the limiting factor in further characterizing the weld process for a range of highly dissimilar materials.

References

1. F. Niklaus, G. Stemme, J.-Q. Lu, and R. J. Gutmann, "Adhesive wafer bonding," J. Appl. Phys. **99**, 031101 (2006).
2. J. Oberhammer, F. Niklaus, and G. Stemme, "Sealing of adhesive bonded devices on wafer level," Sens. Actuators A **110**, 407–412 (2004).
3. A. W. Y. Tan and F. E. H. Tay, "Localized laser assisted eutectic bonding of quartz and silicon by Nd:YAG pulsed-laser," Sens. Actuators A **120**, 550–561 (2005).
4. Q. Wu, N. Lorenz, and D. Hand, "Localised laser joining of glass to silicon with BCB intermediate layer," Microsyst. Technol. **15**, 1051–1057 (2009).
5. H. Huang, L.-M. Yang, and J. Liu, "Ultrashort pulsed fiber laser welding and sealing of transparent materials," Appl. Opt. **51**, 2979–2986 (2012).
6. Y. Ozeki, T. Inoue, T. Tamaki, H. Yamaguchi, S. Onda, W. Watanabe, T. Sano, S. Nishiuchi, A. Hirose, and K. Itoh, "Direct welding between copper and glass substrates with femtosecond laser pulses," Appl. Phys. Express **1**, 82601 (2008).
7. S. Richter, S. Döring, F. Zimmermann, L. Lescieux, R. Eberhardt, S. Nolte, and A. Tünnermann, "Welding of transparent materials with ultrashort laser pulses," Proc. SPIE **8244**, 824402 (2012).
8. W. Watanabe, S. Onda, T. Tamaki, K. Itoh, and J. Nishii, "Space-selective laser joining of dissimilar transparent materials using femtosecond laser pulses," Appl. Phys. Lett. **89**, 021106 (2006).
9. W. Watanabe, T. Tamaki, and K. Itoh, "Ultrashort laser welding and joining," in *Femtosecond Laser Micromachining*, O. Roberto, C. Giulio, and R. Roberta, eds. (Springer-Verlag, 2012), pp. 467–477.
10. P. Kongsuwan, G. Satoh, and Y. L. Yao, "Transmission welding of glass by femtosecond laser: mechanism and fracture strength," J. Manuf. Sci. Eng. **134**, 011004 (2012).
11. T. Tamaki, W. Watanabe, and K. Itoh, "Laser micro-welding of transparent materials by a localized heat accumulation effect using a femtosecond fiber laser at 1558 nm," Opt. Express **14**, 10460–10468 (2006).
12. D. Hélie, M. Bégin, F. Lacroix, and R. Vallée, "Reinforced direct bonding of optical materials by femtosecond laser welding," Appl. Opt. **51**, 2098–2106 (2012).
13. T. Tamaki, W. Watanabe, J. Nishii, and K. Itoh, "Welding of transparent materials using femtosecond laser pulses," Jpn. J. Appl. Phys. **44**, L687–L689 (2005).
14. A. Horn, I. Mingareev, A. Werth, M. Kachel, and U. Brenk, "Investigations on ultrafast welding of glass–glass and glass–silicon," Appl. Phys. **93**, 171–175 (2008).
15. S. Richter, S. Döring, A. Tünnermann, and S. Nolte, "Bonding of glass with femtosecond laser pulses at high repetition rates," Appl. Phys. **103**, 257–261 (2011).
16. K. Sugioka, M. Iida, H. Takai, and K. Micorikawa, "Efficient microwelding of glass substrates by ultrafast laser irradiation using a double-pulse train," Opt. Lett. **36**, 2734–2736 (2011).
17. I. Miyamoto, A. Horn, and J. Gottmann, "Local melting of glass material and its application to direct fusion welding by ps-laser pulses," J. Laser Micro/Nanoeng. **2**, 7–14 (2007).
18. I. Alexeev, K. Cvecek, C. Schmidt, I. Miyamoto, T. Frick, and M. Schmidt, "Characterization of shear strength and bonding energy of laser produced welding seams in glass," J. Laser Micro/Nanoeng. **7**, 279–283 (2012).
19. I. Miyamoto, K. Cvecek, Y. Okamoto, and M. Schmidt, "Novel fusion welding technology of glass using ultrashort pulse lasers," Phys. Procedia **5**, 483–493 (2010).
20. I. Miyamoto, K. Cvecek, and M. Schmidt, "Evaluation of nonlinear absorptivity in internal modification of bulk glass by ultrashort laser pulses," Opt. Express **19**, 10714–10727 (2011).
21. M. F. Ashby and D. R. H. Jones, in *Engineering Materials 2—An Introduction to Microstructures, Processing and Design* (Butterworth-Heinemann, 2006), pp. 202–212.
22. S. M. Eaton, H. Zhang, P. R. Herman, F. Yoshino, L. Shah, J. Bovatsek, and A. Arai, "Heat accumulation effects in femtosecond laser-written waveguides with variable repetition rate," Opt. Express **13**, 4708–4716 (2005).
23. H. A. M. GmbH, "Lap-shear-strength-on-metals," http://www.go-araldite.com/en/component/joomdoc/datasheet/Lap-Shear-Strength-on-metals.pdf/download.